View metadata, citation and similar papers at core.ac.uk
brought to you by CORE
provided by PORTO Publications Open Repository TOrino

Signal Integrity constrained optimization of flexible printed interconnects for mobile devices

S. Grivet-Talocia*, S. Acquadro*, M. Bandinu*, F. G. Canavero*, I. Kelander† and M. Rouvala†
*Politecnico di Torino, Dip. Elettronica, Torino, E-mail: grivet@polito.it
†Nokia Research Center, Helsinki, Finland. E-mail: markku.rouvala@nokia.com

***Abstract*— This paper presents a systematic procedure for optimizing the geometry of high-speed data links based on Signal Integrity constraints. The structures under consideration are flexible printed circuits typically found in mobile devices having moving parts. Since the geometry of such interconnects is approximately translation-invariant, we adopt multiconductor transmission line models, characterized by broadband frequency-dependent per-unit-length parameters that implicitly account for losses and dispersion. Each interconnect is characterized by several geometrical and material parameters, which constitute the free variables for optimization of the link. Signal integrity constraints such as return loss, impedance, attenuation, or ultimately eye diagram opening are used as goals in a closed-loop optimization process. We employ an efficient model parameterization scheme based on the Generalized Method of Characteristics to reduce the number of RLGC computations and to convert the parameterized model into a SPICE-ready deck for transient simulation and eye diagram generation under realistic loading conditions. Several numerical results illustrate the feasibility of the approach.**

I. Introduction

With the continuous increase of complexity, performance, and functionality in portable electronic devices, Signal Integrity aspects have to be taken into account in very early stages of the system design. This applies in particular for high-speed data links that connect the various parts of a mobile device. In this work, we concentrate on a particular class of such interconnects, namely the Flexible Printed Circuits (FPC) typically used in electrical devices to connect electrical modules together in places where flexible or bendable interconnects are advantageous. For example, the interconnect between foldable mobile phone upper block, which has typically a display part, and lower block, which typically has the computing engine part, can be implemented by using a flexible printed circuit going through the hinge structure connecting the two blocks.

FPC interconnections typically have more than one metallic layers, usually copper based materials. Separate single-layer FPCs can indeed be stacked on top of each other, so that there exists so called air gap between each layer (Fig. 1). Each FPC layer must be very thin in order to allow good bendability. However, this small thickness brings challenges to the electromagnetic interference/compatibility (EMI/EMC) design of the interconnect. Typically 30-60 or even more signals are transferred in parallel traces through the FPC. When the transferred data bandwidth is increased, the electrical properties become more and more important in order to maintain good signal quality over the FPC and minimize the unwanted crosstalk between the signals.

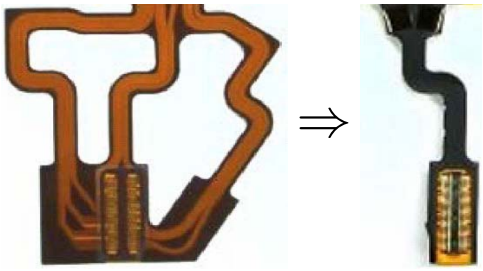

Fig. 1. "Origami style" multilayer FPC (single layer FPC is folded twice).

In the early design phase, the cross-sectional geometry of the interconnect is still to be defined. The manufacturing capabilities set limits to the minimum trace width and gap between traces. On the other hand, transferring as many signals as possible in given width for the FPC is desired. Several main topologies may be available based on the number of layers, and location of signal/ground lines. For each specific class, the actual cross-section is defined by a specific combination of conductor width, separation and height, layer height, and material properties such as dielectric constant and metal conductivity. The main point we want to address in this work is the definition of a procedure for the selection of the optimal cross-sectional geometry once the class of interconnect topology is given.

The cross-section optimization task is based on Signal integrity constraints such as return loss, impedance, attenuation, or ultimately eye diagram opening from transient (SPICE) simulations under realistic driving and loading conditions (possibly nonlinear). It is clear that any multi-dimensional optimization requires several samples in the parameter space. Unfortunately, for present application each of these samples requires: i) a frequency sweep of 2D field solutions for the determination of the RLGC matrices for the geometry under consideration; ii) translation of the frequency-based model specification into a time-domain compatible model which can be analyzed by a standard circuit solver (SPICE); and iii) a possibly long transient simulation in order to compute the eye diagram. The high computational complexity is evident.

In order to reduce the computational cost of the overall optimization run, we adopt a parameterization scheme for macromodels of lossy multiconductor transmission lines based on the so-called Generalized Method of Characteristics [1],

[2]. These models are constructed via extraction of the asymptotic modal delays of the line combined with low-order rational approximations of characteristic admittance and delayless propagation operators. This representation describes the interconnect as a multiport governed by Delayed Ordinary Differential Equation, which can be easily synthesized into an equivalent circuit using only standard elements. The accuracy and efficiency of this macromodeling technique is widely recognized. The proposed parameterization uses suitable interpolation schemes on the residue matrices related to the above-mentioned rational approximations. This procedure results in a significant reduction on the number of RLGC computations, which are only needed on a coarse grid in the parameter space.

The detailed specification of the geometry under investigation is given in Section II. An outline of the model parameterization scheme is provided in Section III. Finally, numerical results and validations are provided in Section IV.

II. Geometry specification

We consider here three different classes of FPC interconnects with one signal layer, depicted in Fig. 2. The three structures differ only for the presence of a bottom and top ground (return) layers and are labeled as type 'A' (no ground layers), type 'B' (only bottom ground layer) and type 'C' (top and bottom ground layers). The signal layer includes four actual signal lines and two lateral ground lines. The geometrical parameters (conductor width w and separation d, dielectric thickness h, etc.) and electrical parameters (dielectric constant ε_r) are specified as ranges of variation, summarized in table I. This is a typical scenario in the early stage of a product development, when the physical design has still to be finalized. All these parameters will be collected in a m-dimensional array $\lambda = (\lambda_1, \ldots, \lambda_m)$.

The interconnect is considered as a uniform transmission line governed by parameterized telegraphers' equations

$$\begin{aligned} -\frac{d}{dz}\mathbf{V}(z,s;\lambda) &= [\mathbf{R}(s;\lambda) + s\mathbf{L}(s;\lambda)]\,\mathbf{I}(z,s;\lambda) \\ -\frac{d}{dz}\,\mathbf{I}(z,s;\lambda) &= [\mathbf{G}(s;\lambda) + s\mathbf{C}(s;\lambda)]\,\mathbf{V}(z,s;\lambda) \end{aligned} \tag{1}$$

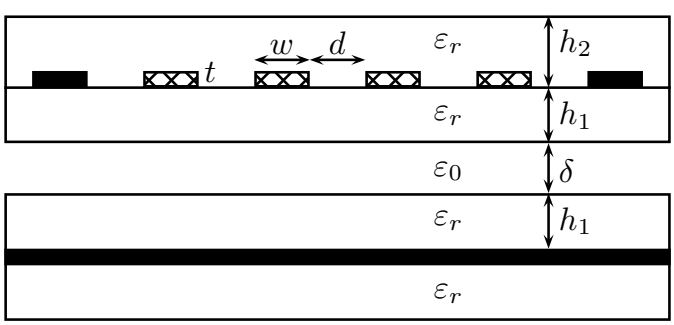

Fig. 2. Cross-section of the (type 'B') transmission-line under investigation with the definition of relevant geometrical/material parameters. Type 'A' is without bottom ground layer and type 'C' has an additional (identical) top ground layer. Crosshatch and solid fill indicate signal and ground conductors, respectively.

where s is the Laplace variable and with $\mathbf{G}(s;\lambda)$, $\mathbf{C}(s;\lambda)$, $\mathbf{R}(s;\lambda)$ and $\mathbf{L}(s;\lambda)$ denoting the frequency-dependent parameterized per-unit-length conductance, capacitance, resistance, and inductance matrices, respectively. We use a Method-of-Moments code based on a combination of the techniques in [3] and [4] for the determination of the per-unit-length matrices once the cross-section is fixed, i.e., for a specific value of the parameter $\lambda = \bar{\lambda}$. In particular, the technique in [3] is employed for the computation of the asymptotic capacitance and inductance matrices $\mathbf{C}(s = \infty; \bar{\lambda})$ and $\mathbf{L}(s = \infty; \bar{\lambda})$, respectively. The technique in [4] is used to compute the frequency-dependent per-unit-length impedance $\mathbf{Z}(j\omega;\bar{\lambda}) = \mathbf{R}(j\omega;\bar{\lambda}) + j\omega\mathbf{L}(j\omega;\bar{\lambda})$ taking into account conductor losses, skin and proximity effects. Dielectric losses were neglected in this preliminary investigation. However, future work will include also dielectric losses since these can be significant due to the broad frequency spectrum of the signals traveling on the interconnect.

III. Parameterized macromodeling scheme

The macromodeling procedure follows from [2], extending all derivations to the parameterized case. A detailed description of this parameterization is available in [7], [8], so only the main steps are highlighted here. The transmission line segment is treated as a multiport, with $\mathbf{V}_1, \mathbf{I}_1$ and $\mathbf{V}_2, \mathbf{I}_2$ denoting the near and far end terminal voltage and current vectors. In the framework of the Generalized Method of Characteristics [5], [2], the solution of Eqs. (1) can be restated as

$$\begin{aligned} \mathbf{I}_1 &= \mathbf{Y}_c(s;\lambda)\mathbf{V}_1 - \mathbf{H}(s;\lambda)\,[\mathbf{Y}_c(s;\lambda)\mathbf{V}_2 + \mathbf{I}_2] \\ \mathbf{I}_2 &= \mathbf{Y}_c(s;\lambda)\mathbf{V}_2 - \mathbf{H}(s;\lambda)\,[\mathbf{Y}_c(s;\lambda)\mathbf{V}_1 + \mathbf{I}_1] \end{aligned} \tag{2}$$

with

$$\begin{aligned} \mathbf{\Gamma}^2(s;\lambda) &= [\mathbf{G}(s;\lambda) + s\mathbf{C}(s;\lambda)]\,[\mathbf{R}(s;\lambda) + s\mathbf{L}(s;\lambda)] \\ \mathbf{Y}_c(s;\lambda) &= \mathbf{\Gamma}^{-1}(s;\lambda)[\mathbf{G}(s;\lambda) + s\mathbf{C}(s;\lambda)] \\ \mathbf{H}(s;\lambda) &= e^{-\mathcal{L}\mathbf{\Gamma}(s;\lambda)} \end{aligned} \tag{3}$$

being the squared propagation matrix, the characteristic admittance matrix, and the propagation operator matrix for a line length $\mathcal{L}$, respectively.

The key point enabling the construction of a macromodel suitable for time-domain analysis will be the approximation of $\mathbf{Y}_c(s;\lambda)$ and $\mathbf{H}(s;\lambda)$ as a combination of rational functions of frequency and pure delay terms. In fact, this approximation

TABLE I
Geometrical and material line parameters.

Parameter	Min	Max
h_1	50 μm	50 μm
h_2	50 μm	65 μm
δ	0 mm	1 mm
w	50 μm	150 μm
d	w	$2w$
t	17.5 μm	17.5 μm
ε_r	3.2	4.0
Length	0 mm	300 mm

leads naturally to a system of Delayed Ordinary Differential Equations, and allows the macromodel to be synthesized into an equivalent circuit using only standard elements.

A. Characteristic admittance operator

All entries of the characteristic admittance matrix $\mathbf{Y}_c(s;\lambda)$ turn out to be very smooth with respect to both frequency and any of the components in λ, i.e., the cross-sectional parameters. Therefore, we consider the approximation

$$\mathbf{Y}_c(s;\lambda) \simeq \sum_n \frac{\mathbf{R}_n^Y(\lambda)}{s-p_n} + \mathbf{Y}_\infty(\lambda) \tag{4}$$

characterized by common poles throughout the parameter space and for each matrix element, and by parameter-dependent residues and direct couplings. Identification of poles and residues follows a three-step procedure:

1) a raw specification of the characteristic admittance matrix is computed via (3) by a frequency sweep of RLGC evaluations over 40 points from almost DC to 10 GHz, with logarithmic spacing. This computation is repeated on a coarse grid of 3 points for each varying geometrical parameter. These grid points in the parameter space are denoted as $\lambda^{(k)}$ in the following;
2) the common poles and the parameter-dependent residues are computed for each of the available parameter configurations $\lambda^{(k)}$, using the well-known Vector Fitting (VF) algorithm [6];
3) a continuous variation throughout the parameter space is recovered as

$$\mathbf{R}_n^Y(\lambda) = \sum_\nu \theta_n^\nu \mathbf{R}_n^Y(\lambda^{(\nu)}), \tag{5}$$

where the coefficients θ_n^ν are determined by multidimensional interpolation. A thorough discussion on the choice of the interpolation scheme is available in [8] and is not repeated here. We remark that linear interpolation is suitable for parameters inducing quasi-linear dependence (ε_r and h_2), spline interpolation is used for w and d/w, since these induce smooth variations, and finally one-pole rational interpolation is used to represent variations induced by the air gap δ.

A few validations of the proposed parameterized rational approximation for the characteristic admittance are reported in Fig. 3. These results correspond to fixed parameter values $\delta = 0.5$ mm, $\varepsilon_r = 3.6$, $h_2 = 57.5\,\mu$m. The conductor width w and separation d/w were considered on a 3x3 grid (minimum, mean, and maximum value for each varying parameter) for the macromodel generation. Upper and lower sets of curves in each panel of Fig. 3 correspond to the two combinations with minimum and maximum values for both w and d/w. Finally, a validation point was selected with $w = 125\,\mu$m, $d/w = 1.75$, the corresponding macromodel was obtained via multidimensional interpolation. Validation of this macromodel responses is provided by the intermediate curves in each panel of Fig. 3. These plots show that (i) the accuracy of the rational approximation is excellent; (ii) the unavoidable errors introduced by the interpolation scheme are almost negligible.

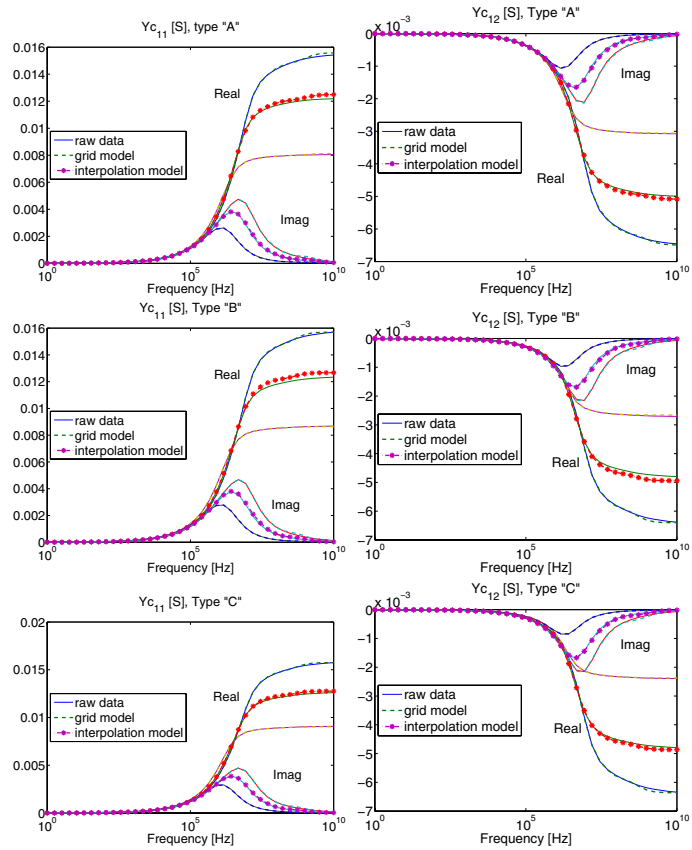

Fig. 3. Validation of the proposed interpolation scheme for two selected entries of the characteristic admittance $\mathbf{Y}_c(s;\lambda)$. In each panel, the upper and lower sets of curves correspond to grid points $\lambda^{(k)}$ in the parameter space where raw data is available. Curves that are inbetween correspond to a validation point for the interpolated model.

B. Propagation operator

The approximation of the propagation operator $\mathbf{H}(s;\lambda)$ follows a slightly different procedure, since this operator includes both pure delay effects (inducing fast phase variations) and attenuation/dispersion effects, which are characterized by slow and smooth variation with frequency. Its direct rational approximation would require a very large number of poles, which would be dependent on the line length. To avoid this difficulty, we attempt the direct extraction of propagation delays, producing a rational approximation of the remaining attenuation/dispersion-dominated operator. Delay extraction is performed in the modal domain, using approximate asymptotic modes in order to simplify the subsequent parameterization and rational approximation. More details follow.

We define a "delayless" propagation operator as

$$\widetilde{\mathbf{P}}(s;\lambda) = \mathrm{diag}\{e^{s\widetilde{T}_k(\lambda)}\}\,\bar{\mathbf{M}}^{-1}\,\mathbf{H}(s;\lambda)\,\bar{\mathbf{M}}\,, \tag{6}$$

where the columns of matrix $\bar{\mathbf{M}}$ provide the high-frequency modal profiles for a "mean" parameter configuration $\lambda = \bar{\lambda}$,

$$\mathbf{\Lambda}(\bar{\lambda}) = \bar{\mathbf{M}}^{-1}\,\mathbf{C}(\infty;\bar{\lambda})\,\mathbf{L}(\infty;\bar{\lambda})\,\bar{\mathbf{M}}\,, \tag{7}$$

with $\mathbf{\Lambda}(\bar{\lambda})$ diagonal. The parameter-dependent approximate

delays in (6) are computed via

$$\widetilde{T}_k(\lambda) = (1-\alpha)\mathcal{L}\sqrt{\Lambda_{kk}(\lambda)}\,. \tag{8}$$

where

$$\mathbf{\Lambda}(\lambda) = \bar{\mathbf{M}}^{-1}\,\mathbf{C}(\infty;\lambda)\,\mathbf{L}(\infty;\lambda)\,\bar{\mathbf{M}}\,. \tag{9}$$

This matrix is not diagonal since the modes are not exact for $\lambda \neq \bar{\lambda}$, but it can be viewed as a small perturbation of the diagonal matrix defined in (7). The parameter α in (8) provides an estimate of this perturbation by computing the maximum modal perturbation throughout the parameter space [8]. In all our tests on several cross-sectional geometries we have always verified that $\alpha < 0.1$, so that the modal perturbation is uniformly small.

The same rational approximation procedure adopted for the characteristic admittance is applied to the delayless operator $\widetilde{\mathbf{P}}(s;\lambda)$. Since most of the delay terms have been extracted, this operator results quite smooth with respect to frequency and requires a small number of poles (typically 10-14). In addition, since "mean" modal profiles are used in its definition, the variations of $\widetilde{\mathbf{P}}(s;\lambda)$ throughout the parameter space λ are also smooth and of the same type of $\mathbf{Y}_c(s;\lambda)$. Therefore, the same interpolation schemes already adopted for $\mathbf{Y}_c(s;\lambda)$ are employed also for $\widetilde{\mathbf{P}}(s;\lambda)$. Finally, the true propagation operator is recovered as

$$\mathbf{H}(s;\lambda) = \bar{\mathbf{M}}\,\mathrm{diag}\{e^{-s\widetilde{T}_k(\lambda)}\}\,\widetilde{\mathbf{P}}(s;\lambda)\,\bar{\mathbf{M}}^{-1}\,. \tag{10}$$

A few validations for the rational fit and interpolation scheme of the delayless propagation operator $\widetilde{\mathbf{P}}(s;\lambda)$ are reported in Fig. 4. These results were obtained following the same procedure already adopted for the validation of the characteristic admittance. See the above discussion in Sec. III-A and Fig. 3. We remark that these plots confirm the quite low sensitivity of the delayless propagation operator with respect to the cross-sectional geometry. This was expected since this operator mainly represents frequency-dependent attenuation and dispersion effects, which have a very weak dependence on the specific geometry configuration.

IV. Optimization and Sensitivity Analysis

We consider in this section some issues related to the optimization process enabling the selection of the optimal cross-sectional geometry that guarantees the best Signal Integrity of the transmission link. In abstract notation we would like to solve the following optimization problem

$$\lambda^{\mathrm{opt}} = \mathrm{argmin}_{\lambda} F(\lambda)\,, \tag{11}$$

where the goal function $F(\lambda)$ quantifies the signal degradation effects due to the imperfect link. The choice for this goal function is critical for the success of the entire procedure. Possible criteria can be based on

- Return loss magnitude over a desired bandwidth
- Impedance level over a desired bandwidth
- Attenuation/dispersion effects
- Eye diagram opening under realistic driving/loading conditions

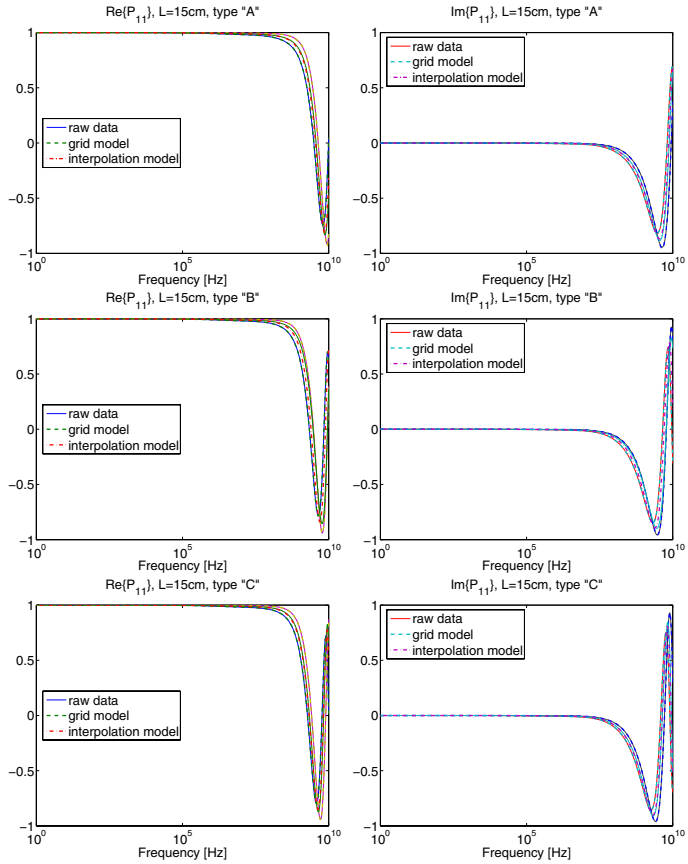

Fig. 4. Validation of the proposed interpolation scheme for a selected entry of the delayless propagation operator $\widetilde{\mathbf{P}}(s;\lambda)$. As in Fig. 3, the upper and lower sets of curves in each panel correspond to grid points $\lambda^{(k)}$ in the parameter space where raw data is available. Curves that are inbetween correspond to a validation point for the interpolated model.

Practically, a combination of the above criteria may be desirable. In this preliminary investigation, we consider only the eye opening. This aspect is probably the most relevant for high-speed digital transmission, since it can be immediately related to safe signaling based on the characteristics of the employed receiver at the line far end.

The first aspect we investigate is the sensitivity of the eye opening to parameter variation. For this analysis we fix the termination scheme as depicted in Fig. 5. All driver resistances are identical, $R = 50\,\Omega$, and all load capacitances are set to $C_L = 1$ pF. Two different driving conditions are considered:

- Single-ended signaling on line k with quiet neighboring lines. This is realized by setting $v_k(t)$ to a pseudo-random bit sequence with $v_n(t) = 0$ for $n \neq k$.
- Single-ended signaling on line k with "worst-case" crosstalk. This is realized as above, but with synchronous aggressors $v_n(t)$ set to a clock signal with the same frequency.

We tested various data rates from 0.5 to 2 Gbps, with a rise time set to 30% of the bit time. All eye diagrams were obtained by running the parameterized macromodel with SPICE, using a total of 500 bits. In all cases the voltage swing of the digital

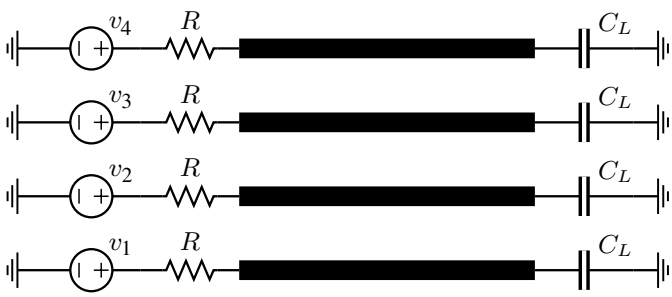

Fig. 5. Termination scheme for the generation of the eye diagram.

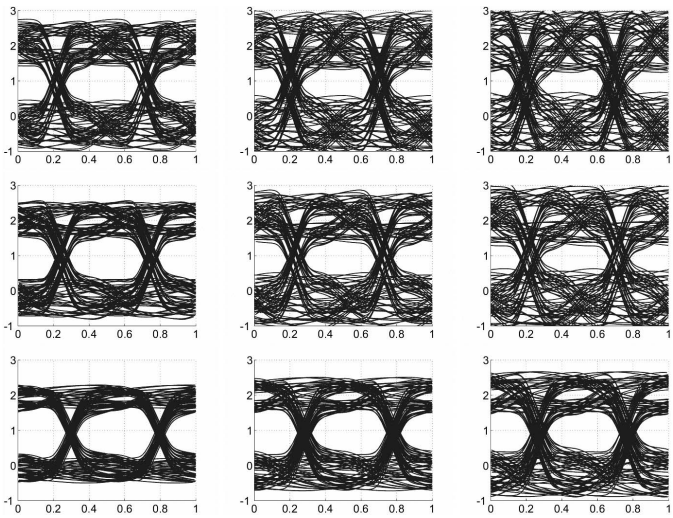

Fig. 6. Transmission eye sensitivity for the quiet aggressors case, with single-ended signaling at 0.5 Gbps on a 30 cm interconnect. Rows from top to bottom correspond to d/w=2, 1.5, and 1 respectively. Columns from left to right correspond to $w = 50,\ 100,\ 150\mu$m, respectively. Horizontal axis is normalized to twice the bit time. Vertical axis is voltage in Volts.

and clock pulses was set to 1.8 V, and no jitter was applied. Note that no clamps were included in the terminations.

Figure 6 shows several different eye diagrams for various geometrical configurations (see caption for details) in the quiet aggressors case, while Figure 7 presents the same eye diagrams for the synchronous clock aggressors case. These plots collectively illustrate the eye sensitivity with respect to the geometrical parameters w and d/w, providing a visual indication on the particular combination of parameters that gives the best eye opening. We remark that, for present investigation, the terminations were kept fixed as in Fig. 5 over the parameter space. Therefore, the main reason for the large sensitivity of the eye opening is probably the parameter-dependent mismatch that is caused by the change in the impedance level of the interconnect when w and d/w are varied. Crosstalk from synchronous aggressors is instead the obvious reason for the eye diagram degradation in Fig. 7.

In order to make these considerations more quantitative, an automated measure of the eye opening is required. When this is available, the measured opening can be inserted as a goal into a multidimensional optimization loop that will output the optimal configuration. Such a measure can be obtained

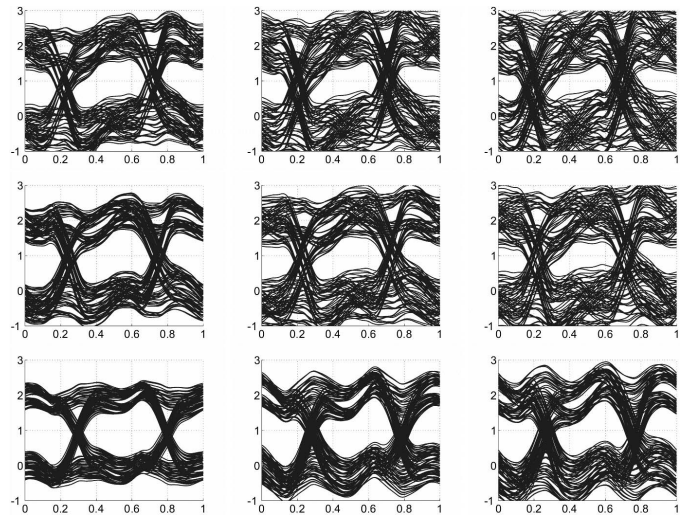

Fig. 7. Transmission eye sensitivity for the worst (synchronous clock) aggressors case, with single-ended signaling at 0.5 Gbps on a 30 cm interconnect. Rows from top to bottom correspond to d/w=2, 1.5, and 1 respectively. Columns from left to right correspond to $w = 50,\ 100,\ 150\mu$m, respectively. Horizontal axis is normalized to twice the bit time. Vertical axis is voltage in Volts.

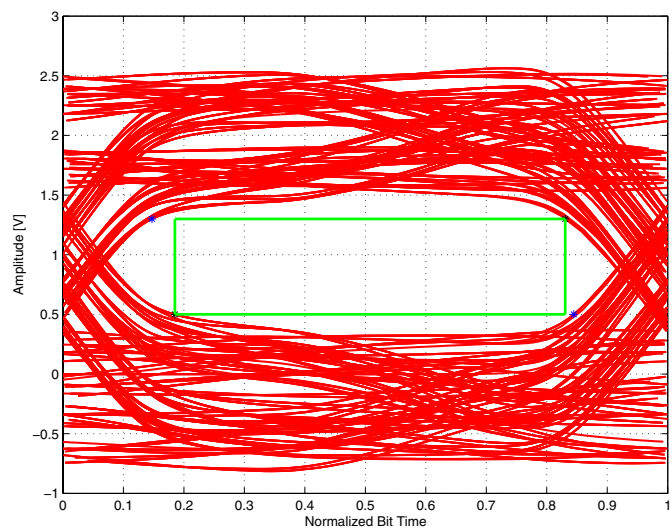

Fig. 8. Graphical illustration of the horizontal eye opening measurement.

as depicted in Fig. 8. The vertical opening is fixed a priori based on the receiver threshold voltage (in this case we use $V_{\rm th} = 0.9$ V) extended by a safety margin (in this case $\Delta V = 0.4$ V). Then, the intersections between all crossing fronts and the two voltage levels $V_{\rm th} \pm \Delta V$ are computed and the horizontal opening is determined as the worst case.

The systematic application of the above procedure to the results of repeated SPICE runs on the proposed parameterized line macromodels constitutes the basis of the proposed link optimization process. In order to avoid running an excessive number of cases for a very fine sampling of the parameter space, we consider an additional assumption of smooth dependence of the horizontal eye opening with respect to each indi-

vidual geometrical parameter. We verified this assumption for several test cases. This allows to perform a limited number of SPICE runs on few prescribed geometries, leading to a coarse representation of the eye opening in the parameter space. Then, smooth interpolation schemes (e.g., spline) are applied directly on the eye opening metric in order to select any necessary additional parameter combinations to be scanned by additional SPICE runs. The process is then iterated. The optimization run completes when the global maximum has been found.

We show the results of the proposed optimization scheme on a test case. All geometry and material parameters are fixed to $\delta = 0.5$ mm, $\varepsilon_r = 3.6$, $h_2 = 57.5\,\mu$m. The conductor width w and separation d/w are free parameters. A 3×3 grid in the two-dimensional parameter space is used to compute the RLGC parameters of the interconnect, which is assumed to be 30 cm long. These are the raw data which are fed to the proposed parameterization scheme. For this test, we match the far end of all lines by inserting additional 50Ω resistors in parallel to the load capacitances of Fig. 5. The receiver threshold voltage and the safety margin are scaled accordingly. For this example, only 25 SPICE runs were performed using the parameterized macromodels of the transmission line. The results are shown in Fig. 9. Top and bottom panels report the horizontal eye opening computed as a fraction of the bit time, as a function of w and d/w, for a bit/rate of 0.5 and 2 Gbps, respectively. The results show that, in this case, the best geometrical configuration is obtained with the largest conductor width w and with minimal separation d/w.

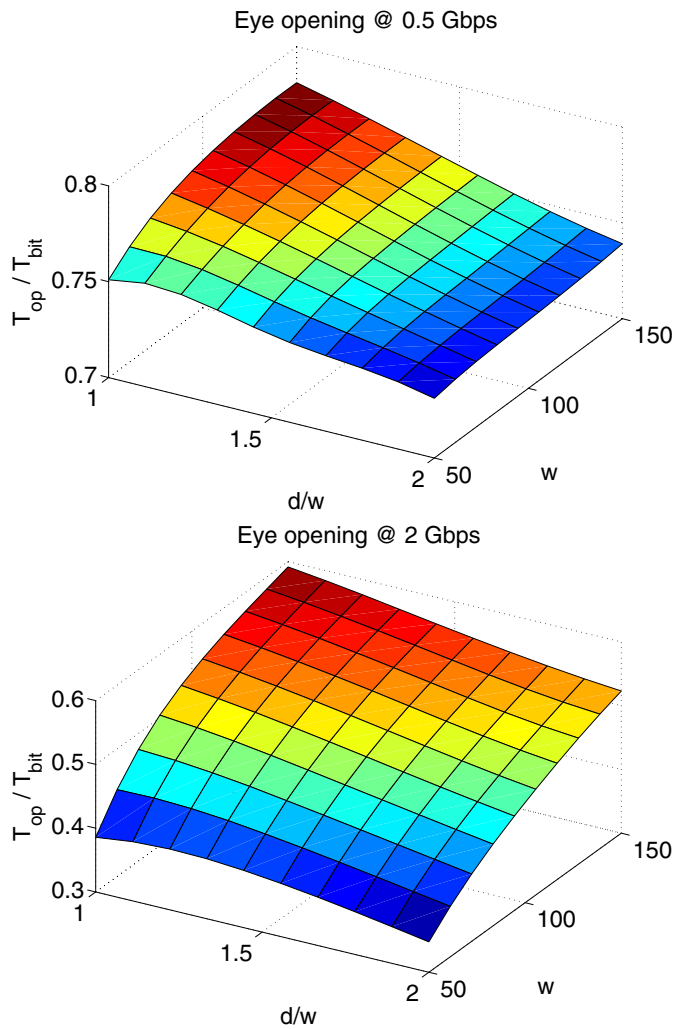

Fig. 9. Horizontal eye opening as a function of the free optimization parameters w and d/w.

V. Conclusion

We have presented a systematic procedure for the determination of the optimal cross-section of a flexible printed interconnect based on Signal Integrity constraints. The horizontal eye opening is considered as the main metric for optimization. This eye opening is computed via repeated SPICE runs on different interconnect models, each corresponding to a particular geometrical configuration. In order to reduce the computational cost of the overall optimization run, we use an efficient parameterization scheme for transmission-line macromodels based on parameterized rational approximations and modal delay extraction. This leads to a compact representation of the electrical behavior of the interconnect in terms of few common poles and parameter-dependent residue matrices. This representation is ideally suited for SPICE analysis at each step of the optimization process. The feasibility of the approach was demonstrated on some flexible printed interconnect cases typically found in high-performance mobile devices.

References

[1] S. Grivet-Talocia, F. G. Canavero, "TOPLline: a delay-pole-residue method for the simulation of lossy and dispersive interconnects", in *Digest of Electr. Perf. Electronic Packaging*, Vol. 11, Monterey, CA, October 2002, pp. 359–362.

[2] S. Grivet-Talocia, H. M. Huang, A. E. Ruehli, F. Canavero, I. M. Elfadel, "Transient Analysis of Lossy Transmission Lines: an Effective Approach Based on the Method of Characteristics" , *IEEE Trans. Advanced Packaging*, pp. 45–56, vol. 27, n. 1, Feb. 2004.

[3] C. Wei, R. F. Harrington, J. R. Mautz, T. Sarkar, "Multiconductor Transmission Lines in Multilayered Dielectric Media", *IEEE Trans. Microwave Theory and Techniques*, Vol. 32, N. 4, Apr. 1984, pp. 439–450.

[4] K. M. Coperich, J. Morsey, V. I. Okhmatovski, A. C. Cangellaris, A. E. Ruehli, "Systematic development of transmission-line models for interconnects with frequency-dependent losses" *IEEE Trans. Microwave Theory and Techniques*, Vol. 49, N. 10, Oct. 2001, pp. 1677–1685.

[5] F. H. Branin, "Transient Analysis of Lossless Transmission Lines", *Proc. IEEE*, Vol. 55, 1967, pp. 2012–2013.

[6] B. Gustavsen, A. Semlyen, "Rational approximation of frequency domain responses by vector fitting", *IEEE Trans. Power Delivery*, Vol. 14, 1999, pp. 1052–1061.

[7] S. Grivet-Talocia, S. Acquadro, C. Peraldo, F. Canavero, I. Kelander, M. Rouvala, A. Arslan, "Parameterized Macromodels for Lossy Multiconductor Transmission Lines", in *17th International Zurich Symposium On Electromagnetic Compatibility*, Feb. 27–Mar. 3, 2006, Singapore, pp. 93–96.

[8] S. Grivet-Talocia, S. Acquadro, C. Peraldo, F. Canavero, I. Kelander, M. Rouvala, "Parametric Macromodeling of Flexible Printed Interconnects for Mobile Devices", accepted in *EMC Europe 2006, International Symposium on Electromagnetic Compatibility*, Sept. 4–8, 2006, Barcelona, Spain.